Journal of
Computational and Theoretical Nanoscience
Vol. 6, 41–45, 2009

Atomistic Simulations of the Nonlinear Deformation and Damage Modes of Super Carbon Nanotubes

Yuli Chen[1], Yajun Yin[1,*], Yonggang Huang[2], and Keh-Chih Hwang[1]

[1] *FML, Department of Engineering Mechanics, Tsinghua University, Beijing 100084, P. R. China*
[2] *Department of Civil and Environmental Engineering and Department of Mechanical Engineering, Northwestern University, Evanston, Illinois 60208, USA*

The tensile deformations and fractures of super carbon nanotubes (STs) are investigated through the atomic-scale finite element method. STs generated from carbon nanotubes (CNTs) with different characteristic aspect-ratioed arms are found to have different nonlinear behaviors in the uniaxial tension process. Specifically, the ST with higher aspect-ratioed arms has three distinct stages: rotation, stretch and rupture, while the ST with lower aspect-ratioed arms has only two stages. Moreover, the local buckling can be only observed in the ST with higher aspect-ratioed arms. This information may lay the foundations for further explorations to the properties of STs in the near future.

Keywords: Super Carbon Nanotube, Y-Branched Carbon Nanotube, Nonlinear Deformation, Damage Mode.

RESEARCH ARTICLE

1. INTRODUCTION

In 1995, Zhou et al. observed branched CNTs with L, Y and T patterns in experiments.[1] Now these carbon nanostructures have been used as multi-terminal electronic devices and circuits.[2,3] Among them, Y-branched CNTs have drawn intense attentions,[4–13] because their symmetrical structures are possible to act as new nanotube-based networks.[14–15]

On the basis of symmetric Y-branched CNTs, a novel carbon nanostructure called super carbon nanotube (ST) is published recently.[16,17] A super carbon nanotube may be generated through replacing the carbon–carbon bonds and carbon atoms of a carbon nanotube respectively by smaller carbon nanotubes and Y-branched junctions.[16] Yin et al.[17] theoretically prove that spontaneous Y-branched CNTs may have both minimum energy and symmetric geometry.

Such beautiful carbon nanostructures have drawn the attentions of researchers. Pugno[18] studied the mimicking nacre with STs for producing optimized super-composites. Wang et al.[19] simulated the mechanical properties of the super graphite (SG), from which STs may be made. Qin et al.[20] predicted the superior flexibility of the STs through molecular dynamics simulations. However, few people explored the influences of the aspect ratios of CNT on the global deformation and damage modes of STs. In this letter, we will try to compensate this weak point by the atomic-scale finite element method (AFEM).[21,22]

2. SIMULATION MODEL

There are three types of CNTs—zigzag, armchair and chirality. Theoretically there are also three types of STs, each of which might be formed by three types of common CNT "arms" and corresponding Y-branched junctions. Hence, there are totally nine types of topologies for the STs. In 1992, Scuseria[4] proposed a kind of symmetric Y-branched junction with armchair topology, which composed of heptagons at the connected junction (Fig. 1(a)). If the armchair CNTs are connected with the Scuseria-type Y-branched junctions, the STs with armchair–chirality (Fig. 1(b)), armchair–armchair (Fig. 1(c)) and armchair–zigzag (Fig. 1(d)) topologies may be formed. In this letter, STs with armchair–zigzag topology will be studied.

The Y-branched CNT (Figs. 2(b and c)) may be considered as the representative cell element for the SG. As reported by Wang et al.,[23] the mechanical properties of the graphite sheet are similar to that of the CNT. Analogously, the mechanical properties of the ST may be very near to that of the SG. If the behaviors of Y-branched CNT (Fig. 2(c)) are clearly understood, the mechanical properties of the STs may be evaluated. Therefore, the

*Author to whom correspondence should be addressed.

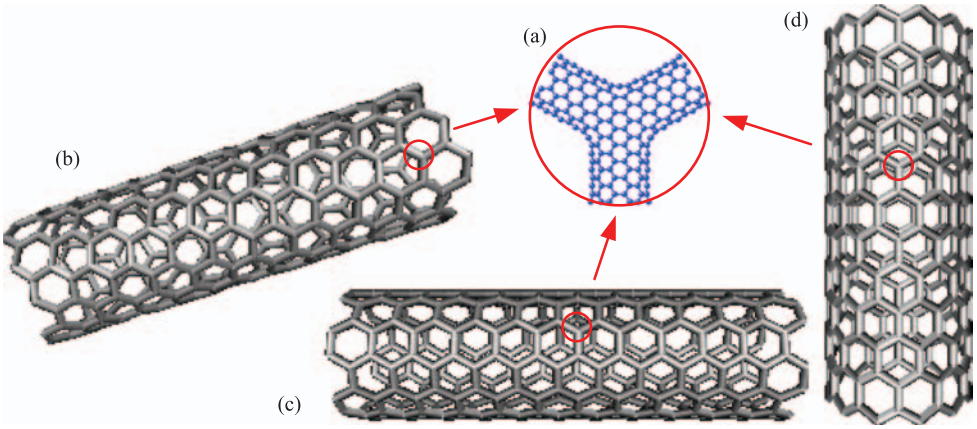

Fig. 1. Super carbon nanotube with Scuseria-type Y-branched junctions: (a) Scuseria-type Y-branched junction, (b) armchair–chirality topology, (c) armchair–armchair topology, and (d) armchair–zigzag topology.

Y-branched CNT or the representative cell element in Figure 2(b) will be focused.

If the arm length of CNTs in the ST is l, the arm length of the Y-branched CNT in the cell element may be $l/2$. The length and width of the cell element may be $\sqrt{3}l$ and $3l/4$ respectively (Fig. 2(b)). The atomic model is presented in Figure 2(c). The Y-branched CNTs are constituted by Scuseria-type junctions and (6, 6) CNTs. Two typical aspect ratios (l/d) are taken as 3 and 6 respectively. The uniaxial tension force F is applied along direction 1. The end of the lower arm is tensioned downward by force F, and the ends of the two upper arms are loaded upward by force $F/2$. The displacements along direction 2 are free from constraint. In the AFEM,[21–22] the modified second-generation Brenner potential[24] and Lennard-Jones 6–12 potential are selected to describe the energies of C–C covalent bonds and Van der Waals interactions respectively.

Figure 3 shows two typical nonlinear deformation and damage processes of the cell element (Figs. 3(a and b)). They are analyzed respectively as follows.

3. NONLINEAR DEFORMATION AND DAMAGE PROCESSES

3.1. Super Carbon Nanotube with High Aspect-Ratioed Arms

When the aspect ratio is not too low ($l/d = 6$), three stages are revealed in the deformation and damage processes (Fig. 3(a)). The first stage ranges from point A to point B, which is a perfect linear line with small slope. The slope is low, because the large aspect ratio may lead to low rigidity of the cell element. Thus the tension force increases slowly along with the increment of the strain. In this stage, the two upper arms look like two "beams" jointed by the junction, and this junction can be viewed as a spiral spring since the angle constraint due to the covalent bonds and Van der Waals interactions among atoms are not rigid. In addition, the two "beams" mainly bear bending deformations. If we carefully check the profile of the two "beams," we may find little stretching deformations but large bending deformations and intensive rotations relative to the vertical symmetric axis. However,

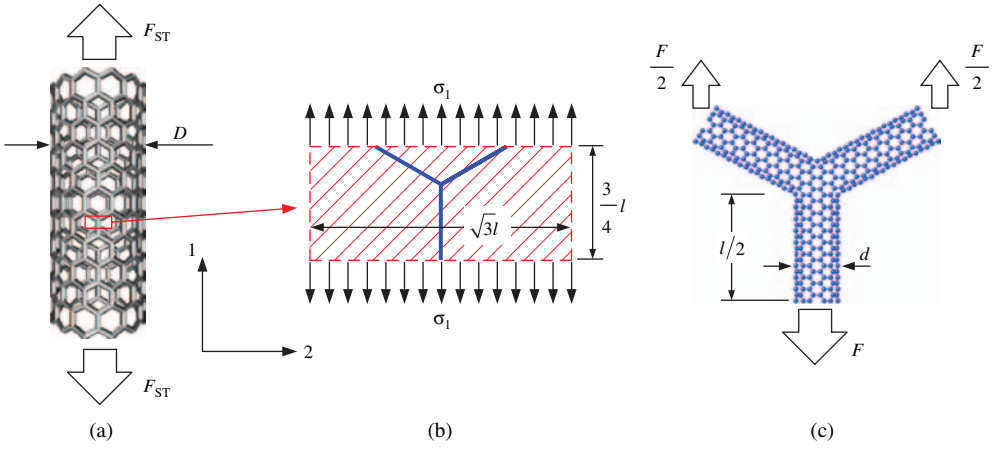

Fig. 2. Simulation model for super carbon nanotube with armchair–zigzag topology: (a) super carbon nanotube under uniaxial tension, (b) the representative cell element of the super carbon nanotube, and (c) the atomic model for AFEM simulations.

RESEARCH ARTICLE

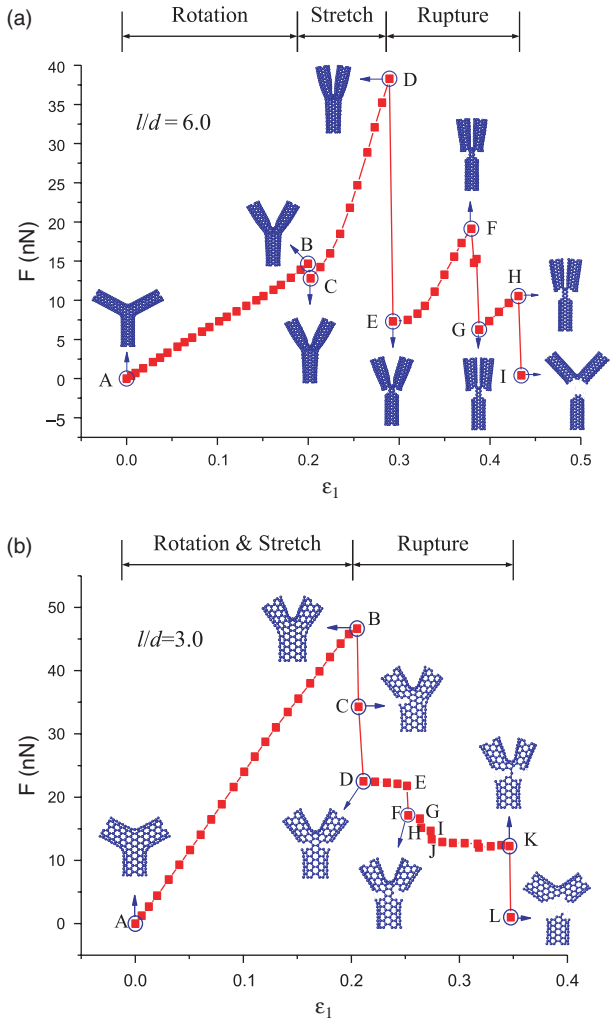

Fig. 3. Typical nonlinear deformation and damage processes of Y-branched CNT: (a) $l/d = 6$ and (b) $l/d = 3$.

the above deformation mode can not be continued forever. If the two upper arms move near enough, their rotations may be baffled by the covalent bonds and Van der Waals interactions among atoms, and visible local deformations near the center of the Y-branched junction appear. At point B with $\varepsilon_B \approx 20.0\%$ and $F_B \approx 14.7$ nN, the first stage is ended.

After the point B, there is the point C with $\varepsilon_C \approx 20.3\%$ and $F_C \approx 12.8$ nN. From B to C, a slight but sudden drop in force is observed. If we carefully check the local deformation around the junction, we may find that this sudden fluctuation in force exactly corresponds to the drastic change in local equilibrium configuration or local shapes near the center of the junction. In mechanics, we know that the transition of equilibrium configurations or deformation modes marks bifurcation or buckling. Therefore, the slight but sudden drop in force is related to the local buckling of the Y-branched junction, and point B may be regarded as the critical point for local buckling.

From point C to point D, we get the second stage of the deformation curve. In this stage, the slope increases suddenly, i.e., there is a sudden hardening transition from the first stage to the second one. This hardening effect may be annotated as follows: Because of the buckling, the angle between the two upper arms starts to become smaller and smaller, which at once leads to the transition in load-carrying mode—The bending-dominant-deformation mode in the first stage is converted into the stretching-dominant-deformation mode in second stage, although the resistance to rotations still exists. Therefore, the hardening effect and large slope may come from both the stretch of the arms and the resistance of the Y-branched junction to the angle change. When the deformation reaches point D, the two upper arms are almost parallel to the lower one, and the tension force approaches the maximum value ($F_{max} \approx 38.3$ nN). The second stage stops at the point D with $\varepsilon_D \approx 28.9\%$ and $F_D = F_{max} \approx 38.3$ nN.

From point D, the third deformation stage is initiated. This stage is very complicated. It includes a few deformation periods. In every period there are two deformation steps. Some of the steps are accompanied by the changes of topologies or ruptures in the Y-branched junction. The first period is D → E → F. The point D is a critical point where the initial rupture occurs: The bonds begin to break symmetrically from the both sides of the Y-branched junction. After the initial rupture, the force suddenly drops to point E with $\varepsilon_E \approx 29.3\%$ and $F_E \approx 7.3$ nN. This sudden drop comes from the continuous breakages of bonds and the propagations of a pair of symmetric cracks from the both sides to the center of the junction. Because the strain increases very little from D to E during the drop, we may deduce that the breakages of bonds appear swiftly or almost simultaneously, and the ruptures of the cracks are brittle. In another word, the pair of the cracks may propagate unstably. Fortunately, this unstable propagation can not be progressed forever. There is a mechanism of brake to the propagations of the cracks: At point E, the breakage of bonds and the propagation of cracks are stopped, and another step, i.e., E → F, occurs. The E → F step is a reloading and hardening one inside which stretching deformations in the arms and the necked region between two cracks are developed. In this step, no breakage of bonds and change in topology occur. The D → E → F forms a complete fracture and deformation period. Point F is also a critical point from where another complete fracture and deformation period F → G → H is started. From point H, the last period begins. However, this period is not finished, because the remained bonds are penetrated by the tips of the two cracks, and the Y-branched CNT is separated into two parts at point I, which finally ends the third stage. It is noted that the succeeding periods become shorter and shorter, because the remained number of load-carrying bonds become smaller and smaller.

At last, the profile of the deformation curve in the third stage is of the wave-like or "zigzag" style. In

appearance this stage is composed of a series of "sudden unloading → reloading → sudden unloading → reloading" transitions. Practically this stage includes a series of transitions from "sudden softening → hardening" and "dynamic cracking → static stretching."

3.2. Super Carbon Nanotubes with Low Aspect-Ratioed Arms

When the aspect ratio is very low ($l/d = 3$), only two stages are disclosed in the deformation and damage processes (Fig. 3(b)). The first stage ranges from point A to point B, and is also a perfect linear stage with large slope. It is interesting to note that there is no obvious transition between rotation and stretch stages as in the previous high aspect-ratio case, since both two deformation modes (rotation and stretch) are comparable and develop simultaneously in low aspect-ratio case. More specifically, the rigidity of the cell element with low aspect-ratioed arms is large, and both the bending deformation and the rotation become difficult. The first stage is finished at point B, and the force reaches the maximum value $F_B = F_{max} \approx 46.7$ nN and the strain approaches $\varepsilon_B \approx 20.5\%$. To one's surprise, during the linear deformation stage, there is no local buckling at the junction, which is very different from the deformation modes shown in Figure 3(a). Hence the aspect ratio strongly affects the deformation modes of the Y-branched junction and the ST.

The second stage starts from point B. It also includes a few characteristic periods. Inside each period there are a few characteristic steps. Here we will concentrate on the first period B → C → D → E in which steps B → C, C → D and D → E are included. Point B is also a critical point for initial fracture. The step B → C corresponds to a sudden drop in force (from $F_B \approx 46.7$ nN to $F_C \approx 34.3$ nN). If we carefully check the topology of the junction, we may find that this drop corresponds to the breakage of bonds and the propagation of crack. The breakage and crack propagation initially occur from one side (left side in Fig. 3(b)) of the junction. At critical point C, the left crack propagation stops, and there is another sudden drop in force in C → D (from $F_C \approx 34.3$ nN to $F_D \approx 22.5$ nN). However, this drop is not caused by the left crack, but is induced by the new one—The right crack is created and developed by the breakages of bonds from the right side of the junction. At point D, the propagation of the right crack is stopped. At the same time, the left crack and the right one reach balance and form a symmetric profile. In the step D → E, we find an almost horizontal deformation curve or a platform in which the force keeps unchanged but the strain grows swiftly. During this process, the balanced pattern of the two cracks and the symmetric topology of the cell element are kept unchanged, but the distortions of the remained hexagons induced by pure stretching deformations between the two cracks are clearly observed. At point E, the period B → C → D → E with a "L" shaped contour is ended. From point E, a new period E → F → G → H → I → J → K is started. This process continuously repeating until the full breakage occurs.

4. CONCLUSIONS

In summary, the two representative nonlinear processes simulated by the atomic-scale finite element method in Figures 3(a and b) reveal plentiful information about the deformation and damage of Y-branched junction and ST under uniaxial tension. Several significant differences between the Y-branched STs with larger aspect-ratioed arms in Figure 3(a) and smaller ones in Figure 3(b) are found:

(i) the former has three distinct stages: rotation, stretch and rupture, while the latter has only two stages because the rotation and stretch stages are merged;

(ii) the local buckling takes place before the bond breaking in the former case, but not found in the latter case;

(iii) the tension–extension curves after the bond breaking exhibit the zigzag feature in the former case, but exhibit the step-like feature in the latter case.

These differences enrich our knowledge about Y-branched junctions and STs, and may lay the foundations for further explorations to their properties in the near future.

Acknowledgment: Supports by the Chinese NSFC under Grant No. 10572076 and No. 10702034 are gratefully acknowledged.

References

1. D. Zhou and S. Seraphin, *Chem. Phys. Lett.* 238, 286 **(1995)**.
2. L. Chico, V. H. Crespi, L. X. Benedict, S. G. Louie, and M. L. Cohen, *Phys. Rev. Lett.* 76, 971 **(1996)**.
3. M. Terrones, F. Banhart, N. Grobert, J.-C. Charlier, H. Terrones, and P. M. Ajayan, *Phys. Rev. Lett.* 89, 075505-1 **(2002)**.
4. G. E. Scuseria, *Chem. Phys. Lett.* 195, 534 **(1992)**.
5. L. P. Biro, R. Ehlich, Z. Osvath, A. Koos, Z. E. Horvath, J. Gyulai, and J. B. Nagy, *Diamond Relat. Mater.* 11, 1081 **(2002)**.
6. J. Li, C. Papadopoulos, and J. Xu, *Nature* 402, 253 **(1999)**.
7. P. Nagy, R. Ehlich, L. P. Biro, and J. Gyulai, *Applied Physics A-Materials Science & Processing* 70, 481 **(2000)**.
8. B. C. Satishkumar, P. J. Thomas, A. Govindaraj, and C. N. Rao, *Appl. Phys. Lett.* 77, 2530 **(2000)**.
9. B. Gan, J. Ahn, Q. Zhang, S. F. Yoon, Rusli, Q. F. Huang, H. Yang, M. B. Yu, and W. Z. Li, *Diamond Relat. Mater.* 9, 897 **(2000)**.
10. B. Gan, J. Ahn, Q. Zhang, Q. F. Huang, C. Kerlit, S. F. Yoon, Rusli, V. A. Ligachev, X. B. Zhang, and W. Z. Li, *Mater. Lett.* 45, 315 **(2000)**.
11. F. L. Deepak, A. Govindaraj, and C. N. Rao, *Chem. Phys. Lett.* 345, 5 **(2001)**.
12. W. Z. Li, J. G. Wen, and Z. F. Ren, *Appl. Phys. Lett.* 79, 1879 **(2001)**.
13. J. M. Ting and C. C. Chang, *Appl. Phys. Lett.* 80, 324 **(2002)**.
14. M. Terrones, *Annual Review of Materials Research* 33, 419 **(2003)**.
15. S. Dag, R. T. Senger, and S. Ciraci, *Phys. Rev. B* 70 **(2004)**.
16. V. R. Coluci, Galv, D. S. O, and A. Jorio, *Nanotechnology* 17, 617 **(2006)**.
17. Y. Yin, Y. Chen, J. Yin, and K. Huang, *Nanotechnology* 17, 4941 **(2006)**.

18. N. M. Pugno, *Nanotechnology* 17, 5480 **(2006)**.
19. M. Wang, X. Qiu, and X. Zhang, *Nanotechnology* 18, 075711 **(2007)**.
20. Z. Qin, X. Q. Feng, J. Zou, Y. Yin, and S. W. Yu, *Appl. Phys. Lett.* 91, 043108-3 **(2007)**.
21. B. Liu, Y. Huang, H. Jiang, S. Qu, and K. C. Hwang, *Computer Methods in Applied Mechanics and Engineering* 193, 1849 **(2004)**.
22. B. Liu, H. Jiang, Y. Huang, S. Qu, M. F. Yu, and K. C. Hwang, *Phys. Rev. B* 72 **(2005)**.
23. L. F. Wang, Q. S. Zheng, J. Z. Liu, and Q. Jiang, *Phys. Rev. Lett.* 95 **(2005)**.
24. D. W. Brenner, O. A. Shenderova, J. A. Harrison, S. J. Stuart, B. Ni, and S. B. Sinnott, *J. Phys.: Condens. Matter* 14, 783 **(2002)**.

Received: 2 April 2008. Accepted: 10 April 2008.